Polarization Sensing with Resonant Cavity Enhanced Photodetectors

Bora M. Onat, *Student Member, IEEE,* and M. Selim Ünlü, *Senior Member, IEEE*

Abstract— **We describe a new method of sensing the linear polarization of light using resonant cavity enhanced (RCE) photodetectors. The RCE detectors are constructed by integrating a thin absorption region into an asymmetric Fabry–Perot cavity. The top reflector is formed by the semiconductor air interface, while the bottom mirror is a distributed Bragg reflector (DBR). Quantum efficiency of these RCE devices can be controlled by tuning the cavity length by recessing the top surface of the detector. For off-normal incidence of light, the reflectivity of the semiconductor-air interface can be significantly different for TE(s) and TM(p) polarizations. A pair of monolithically integrated RCE photodetectors with cavity lengths tuned for resonance and antiresonance provide a large contrast in response to TE and TM polarizations. An alternative polarization sensor can be formed by vertically integrating a conventional and a RCE photodetector. We show that a large contrast in the TE/TM responsivities of the vertical cavity polarization detectors (VCPD) can be achieved, thus combining detection and polarization sensing in a single mesa semiconductor device. These devices alleviate the problems associated with the bulkiness and critical alignment constraints of the conventional sensors based on polarizing filters or splitters and have potential for fabrication of monolithic smart pixels and imaging arrays.**

I. Introduction

POLARIZATION sensing has various applications ranging from magnetooptical data storage [1] to imaging [2]. In imaging, the polarized light sensitivity is expected to underlie a visual quality similar to color vision that might permit the detection of objects that are blended in the background [3]. In magnetooptical (MO) drives, the content of the stored data is coded as a change in the polarization of light [1]. The conventional MO reading head configuration employ polarizing beam splitters and dedicated detectors for the two polarization components. The use of bulk discrete optical components requires individual alignment in three spatial and three angular coordinates with narrow tolerances, resulting in increasing cost and limited range of applications. Several innovative approaches have been proposed to make the packaging of the optical system simpler and tolerant to alignment variations [4]. Recently, a cascaded holographic sensor element has been proposed [5], but the authors expect this element to be highly sensitive to alignment and wavelength variations. A main consideration of all of these implementations is the problem of having heavy and bulky optical elements which limit access time of the data reading head. It is, therefore, strongly desirable to integrate polarization selectivity and detection in a single semiconductor device structure.

Devices incorporating lateral periodic structures, such as grating couplers and wire grid polarizers, have demonstrated polarization dependence when the periodicity is in the order of the wavelength [6], [7]. Metal-semiconductor-metal (MSM) photodetectors with subwavelength electrode finger dimension have also been shown to exhibit polarization and wavelength sensitivity [6].

Recently, we have described a new photodetector structure sensitive to the polarization of the incident radiation without requiring any external polarization filters or beam splitters [8], [9]. The principle of operation is based on the resonant cavity enhanced (RCE) photodetectors [10] in which the absorption region of the photodetector is placed in an asymmetric Fabry–Perot cavity. For the polarization sensing application, the cavity of the RCE detector is constructed by utilizing the semiconductor air interface as a top reflector and a distributed Bragg reflector (DBR) as the bottom mirror. For off-normal incidence of light, the reflectivity of the semiconductor-air interface (R_1 of the cavity) can be significantly different for TE(s) and TM(p) polarizations, as shown in Fig. 1. At Brewster's angle, for example, TM reflectivity vanishes and TE reflectivity is approximately 0.75 for the GaAs-air interface. Therefore, sensitivity (quantum efficiency) is a strong function of the cavity length for TE polarization and can be controlled by recessing the top surface, while the sensitivity for TM is invariant. A pair of monolithically integrated RCE photodetectors with cavity lengths tuned for resonance and antiresonance for TE polarization provides a large contrast. A comparison of the current from these two detectors under equal illumination yields the polarization of the incident light. For this application, uniform top illumination of both of the detectors is essential. In this paper, we extend the application of RCE detectors in polarization sensing to a vertically integrated structure, thus, removing the need for uniform illumination requirement of an array of devices. In this vertical cavity polarization detector (VCPD) structure, a RCE detector is vertically integrated with a conventional detector. The polarization dependencies of both mirror reflectivities of the cavity, i.e., top (R_1) and bottom (R_2) reflector, are utilized to change the sensitivity of the detectors for TE and TM polarizations.

In this paper, we first briefly describe the formulation of RCE photodetection and dependence of quantum efficiency on mirror reflectivities. Then, an analysis of polarization

Manuscript received April 15, 1996; revised August 9, 1996. This work was supported in part by the National Science Foundation under Grant No. ECS-9309607 and by ONR Grant No. N00014-93-1-1186.

The authors are with Boston University, Center for Photonics Research and Department of Electrical & Computer Engineering, Boston, MA 02215 USA.

Publisher Item Identifier S 1077-260X(96)08127-0.

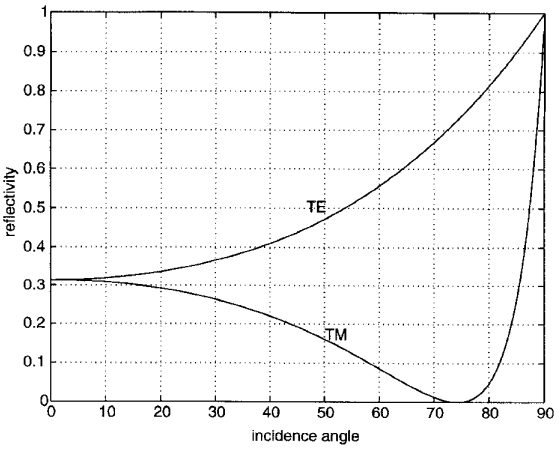

Fig. 1. Polarization dependence of top reflectivity for the GaAs-air interface.

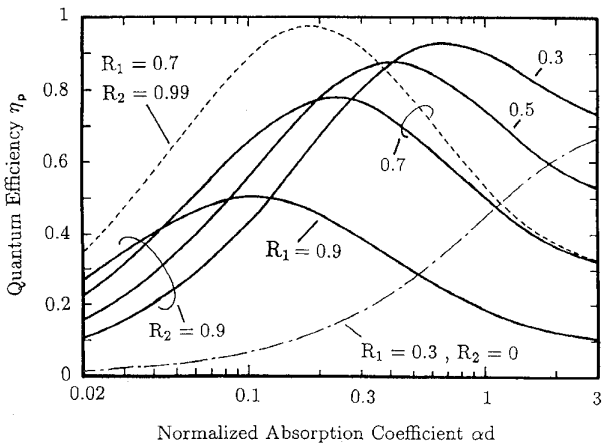

Fig. 2. Calculated η as a function of the normalized absorption coefficient. Solid lines show η at the resonance mode peaks for $R_2 = 0.9$, dashed lines at $R_2 = 0.99$ and $R_1 = 0.7$, and dotted dashed lines the conventional detector case ($R_2 = 0$, $R_1 = 0.3$) (after [10]).

sensing with RCE detector arrays is presented. Finally, the structure and operation principles of the proposed VCPD is discussed. Design considerations are addressed and tolerances due to parameter variations from calculations are shown. The performance of the VCPD is investigated for the GaAs–AlGaAs–InGaAs and Si–SiO_2–Si_3N_4 material systems.

II. RCE Detection

Over the past five years, a new family of optoelectronic devices has emerged whose performance is enhanced by placing the active device structure inside a Fabry–Perot resonant microcavity [10]. The RCE detector structure consists of a thin absorption region placed in an asymmetric Fabry–Perot cavity. The cavity is formed by top and bottom reflectors which can be fabricated by various methods (e.g., alternating layers of quarter-wavelength dielectrics, i.e., DBR's). The RCE devices benefit from the wavelength sensitivity and the large increase of the resonant optical field introduced by the cavity. This results in high quantum efficiencies at optical resonance without requiring thick absorption regions. The quantum efficiency for a RCE detector can be expressed as [10]

$$\eta = \frac{(1 + R_2 e^{-\alpha d})}{1 - 2\sqrt{R_1 R_2} e^{-\alpha d} \cos(2\beta L + \psi_1 + \psi_2) + R_1 R_2 e^{2\alpha d}} \times (1 - R_1)(1 - e^{-\alpha d}) \quad (1)$$

where α and d are the absorption coefficient and thickness for the thin absorber, β is the optical propagation constant, L is the length of the cavity, and R_1, ψ_1, and R_2, ψ_2 are the amplitude and phase of the top and bottom reflectors, respectively. If the light incidence is at an angle θ_{in} with the normal, L is replaced by $L/\cos\theta_{\text{in}}$. For off-normal incidence angles, the reflectivities R_1 and R_2 are a strong function of polarization. Thus, the RCE detector quantum efficiency will be different for TE and TM polarizations.

When the optical length of the cavity satisfies the resonance condition, the cavity enhances the optical fields and the detector response is drastically increased. The peak quantum efficiency η_p is then given by

$$\eta_p = \left\{ \frac{(1 + R_2 e^{-\alpha d})}{(1 - \sqrt{R_1 R_2} e^{-\alpha d})^2} \right\} \times (1 - R_1)(1 - e^{-\alpha d}). \quad (2)$$

If the length of the cavity is altered (e.g., by surface recessing), quantum efficiency can be reduced below that of a conventional detector without the cavity. The enhancement/reduction in the detector response depends strongly on the top reflectivity (R_1) [10].

The origin of the drastic enhancement in η is the greatly increased amplitude of the electric field inside a high Q resonant cavity which causes more energy to be absorbed in the active region. An equivalent interpretation is that an individual photon is multiply-reflected at the mirrors and therefore makes many passes through the absorption region for varying mirror reflectivities as a function of αd. For small thin absorbers ($\alpha d \sim 0.1$), i.e., a low-loss cavity, the enhancement factor exceeds 10.

Fig. 2 shows the quantum efficiency η at resonance as a function of αd for various top (R_1) and bottom (R_2) mirror reflectivities. The conventional case ($R_2 = 0$) is given by a dotted-dashed line. For a native semiconductor surface ($R_1 = 0.3$), the $R_2 = 0$ and 0.9 curves show the contrast between the conventional and RCE cases. RCE detection improves η by a factor of 6.5 for a 0.1-μm thick absorption layer ($\alpha = 10^4$ cm^{-1}). Quantum efficiency can be further enhanced by higher reflectivity mirrors. The $R_2 = 0.99, R_1 = 0.7$ curve reaches a maximum η in excess of 98%.

III. Polarization-Sensing RCE Arrays

Fig. 3 shows a conceptual representation of the polarization-sensitive detector array consisting of two monolithically integrated RCE photodetectors with different cavity lengths (L_1 and L_2). The concepts described below are applicable to most material systems and detector structures at various wavelength (λ) regions. In this section, the discussion will focus on calculations based on a GaAs–AlGaAs–InGaAs photodetector structure designed for an operation wavelength of $\lambda =$

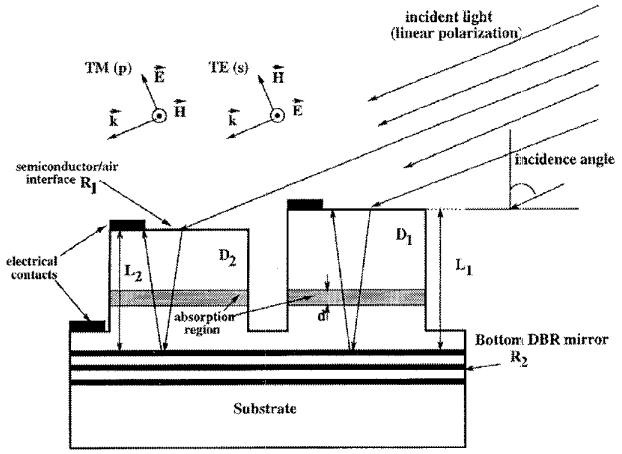

Fig. 3. Conceptual representation of the polarization-sensitive photodetector array consisting of two RCE monolithically integrated photodetectors. A maximum cavity length of $L_{\max} = 2.5$ μm is considered. The length of detector #1 is adjusted to achieve the maximum sensitivity of the resonant cavity for TE polarization for the incidence angle. The surface of detector #2 is recessed such that the incident TE polarized light is rejected. The interface between semiconductor and air is used as the top reflector [6], [7].

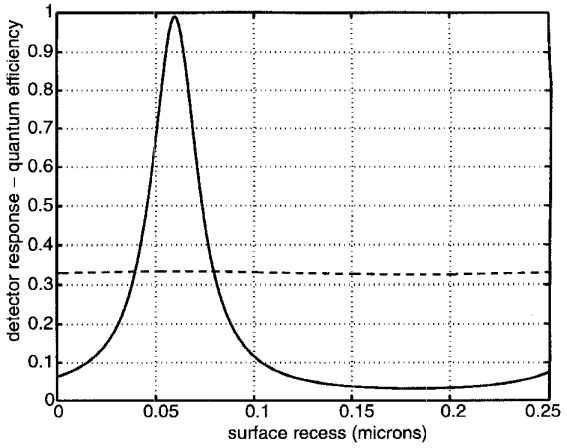

Fig. 4. Dependence of quantum efficiency to surface recess for TE (solid line) and TM (dashed line) for a RCE detector. The wavelength is 900 nm, the incidence angle is 74°, the maximum cavity length of the detector is 2.5 μm, the normalized absorption coefficient αd is 0.2, and an ideal bottom reflector ($R_2 \sim 1$) is assumed.

900 nm. The detector structures consist of an asymmetric Fabry–Perot cavity formed by an AlAs–GaAs DBR bottom mirror ($R_2 \sim 1.0$) and semiconductor-air interface. A thin InGaAs absorption region placed in the GaAs cavity extends the photosensitivity beyond the GaAs absorption edge where optical losses in the other layers are negligible. At around $\lambda =$ 900 nm, only the InGaAs region is absorbing, allowing for the formation of a low-loss resonant cavity.

The interface between semiconductor (GaAs) and air constitutes the top mirror, providing a reflectivity of 0.32 at normal incidence. This reflectivity is a strong function of incidence angle θ_{in} and polarization (Fig. 1). While the reflectivity (R_1) for TE exhibits a monotone increase with increasing θ_{in}, TM reflectivity decreases, vanishing at the Brewster's angle θ_{B} ($\sim$74° for GaAs). For an off-normal incidence angle, therefore, there is a contrast in the response of the RCE detectors to TE and TM polarizations. At $\theta_{\text{in}} = \theta_{\text{B}}$, the detector response is a strong function of the cavity length for TE polarization due to the resonance effect ($R_1 = 0.75$ for TE) and can be controlled by recessing the top surface. On the other hand, the response to TM polarization is invariant since the vanishing top reflectivity eliminates the wavelength dependence due to the RCE effect. Therefore, the detectors D_1 and D_2 in Fig. 3 can be made to have significant contrast in their response to TE polarization while their responses to TM polarization are virtually equal.

Computer simulations based on solving the equations of electromagnetic wave propagation in a planarly stacked dielectric media via a recursive reflection coefficient calculation approach was utilized. The dependence of the detector sensitivities to variations in wavelength, surface recess, and incidence angle was calculated. Fig. 4 shows the calculated dependence of the RCE detector response on the surface recess for TE and TM polarizations. A GaAs–AlGaAs–InGaAs photodetector with as-grown cavity length of $L_{\max} = 2.5$ μm is considered at $\theta_{\text{in}} = \theta_{\text{B}}$. The absorption region is selected to be 0.2-μm thick to maximize the TE detection at resonance. As the cavity length is reduced by recessing the epi-surface, the TE response varies drastically as the detector goes through resonance and antiresonance. The cavity length of detector D_1 (L_1 in Fig. 3) is adjusted to achieve the maximum sensitivity of the resonant cavity for TE polarization for the selected incidence angle. The surface of detector D_2 is recessed such that the incident TE polarized light is rejected. Unlike the large contrast in TE response, these two detectors have nearly identical TM response as indicated by the dashed line in Fig. 4.

Using the same computer simulation program described above, the field distribution and absorption in the entire multilayer structure as well as reflection and transmission coefficients have been computed. The calculated quantum efficiency of both detectors shows a less than 5%/degree variation in the incidence angle around the Brewster's angle. Wavelength dependence is more severe for TE sensitivity for detector D_1 (resonant for TE), and it is about 5%/nm of wavelength variation. The fairly good tolerance of the device performance to variations in angle and wavelength is encouraging. It appears feasible to build polarization-sensing arrays with absolute accuracies within several percent.

Note that it is not necessary to use the Brewster's angle to have a difference between the sensitivity to different polarizations. At any off-normal incidence, TE and TM sensitivities will be different for the two detectors. The contrast will increase with deviation from normal incidence peaking at Brewster's angle.

An important drawback of polarization-sensing detector arrays, utilizing either MSM [6] or RCE arrays [9], is the necessity for uniform top illumination for each of the detectors in the array. Uniform illumination can be achieved by using a spot size much greater than the detector dimension, in which case a large fraction of the incident light will be wasted. Another practical solution is to fabricate arrays consisting of more elements than the minimum requirement of two detectors. A comparison of the photocurrent from several

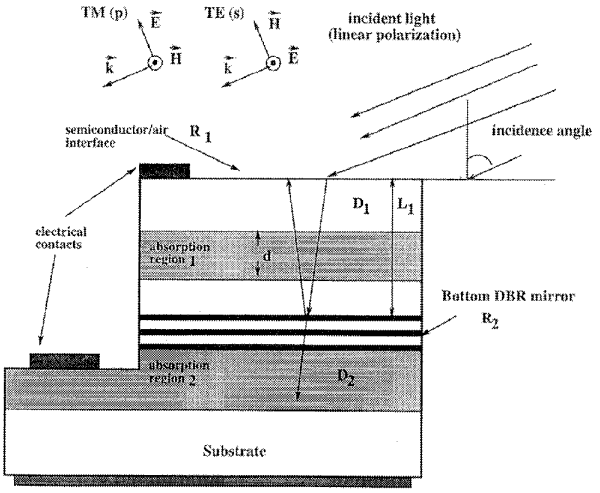

Fig. 5. Conceptual representation of the polarization-sensitive photodetector array consisting of two RCE monolithically integrated photodetectors. The length of detector #1 is adjusted to achieve the maximum sensitivity of the resonant cavity for TE polarization for the incidence angle.

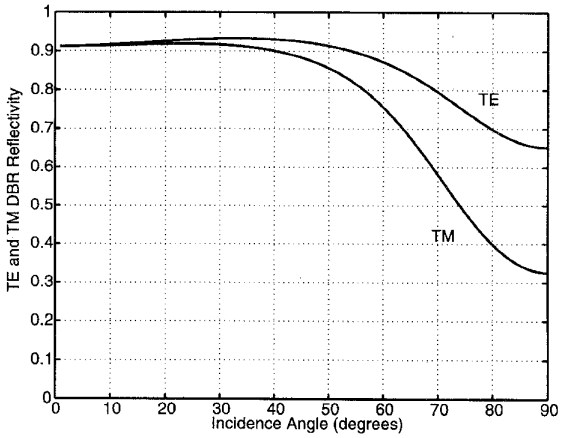

Fig. 6. Reflectivity of the DBR mirror (R_2) for the GaAs–AlGaAs material system for TE and TM polarized light versus incidence angle. Note the contrast in reflectivity at large incidence angles.

detectors with same design can be used to estimate the spatial distribution of light intensity and to correct for the nonuniformities for TE and TM detectors.

IV. Vertical Cavity Polarization Detectors

We describe a new vertical structure to overcome the difficulty associated with the uniform top illumination requirement for multiple detectors for polarization sensing. In this structure, a RCE detector (D_1) is vertically integrated with a conventional detector (D_2) as shown in Fig. 5. We have demonstrated that a large contrast in the TE/TM reflectivity can be achieved for a bottom DBR mirror (R_2) at off-normal incidence. Fig. 6 shows the variation of DBR reflectivity for a 20-period AlAs–AlGaAs DBR mirror with the incidence angle. Since the top reflectivity (semiconductor-air interface) is also polarization-dependent, the resulting cavity provides resonance enhancement for TE, capturing the TE polarized light in the top

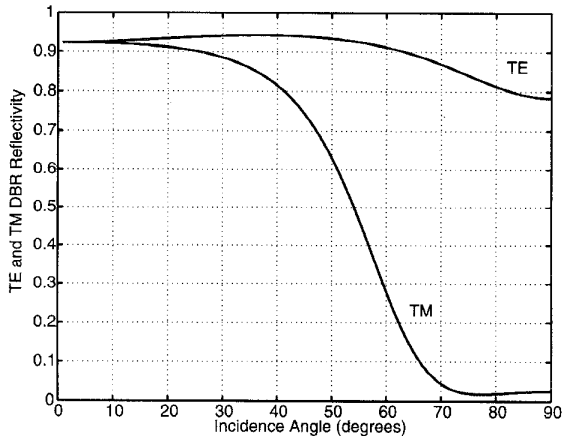

Fig. 7. Reflectivity of a five-period DBR mirror (R_2) for the Si–SiO_2–Si_3N_4 material system for TE and TM polarized light versus incidence angle. Note the significant contrast in reflectivity at large incidence angles.

detector (D_1). For TM, both reflectivities are small, therefore, light is transmitted to the bottom detector (D_2). For a thin absorbing layer in the RCE detector (D_1 in Fig. 5), a large contrast in TE/TM response of D_1 and D_2 is achieved and the linear polarization can be computed from their relative responses.

The contrast in the TE/TM reflectivity of the bottom DBR mirror is relatively small for an AlAs–AlGaAs structure since the incident beam is strongly refracted due to the large refractive index ($n = 2.9$ for AlAs). The beam inside the semiconductor is therefore always at a small angle with the normal, resulting in a small difference in reflectivities at the AlAs–AlGaAs interfaces. The DBR reflectivity contrast can be improved significantly if smaller refractive index materials are used to construct the multilayer structure. For the GaAs material system, the use of native oxide mirrors (with n as small as 1.7) [11] represents a promising alternative. Implementing smart pixels for the GaAs–AlGaAs–InGaAs material system may be achieved by the monolithic integration of the VCPD structures with GaAs VLSI circuitry. Extra epitaxial layers needed to form the top VLSI circuitry may be grown on top of the VCPD structure. Once the circuit fabrication is completed, the mesa of the VCPD may be revealed via etching. Finally, the VCPD and the electronic circuitry can be connected during the last metallization process for evaluation of the two detector outputs to compute the incident polarization.

Implementation of the VCPD in the Si material system with dielectric DBR mirrors offers a more drastic enhancement in the contrast. For a SiO_2–Si_3N_4 DBR, a large contrast in bottom mirror reflectivity (R_2) for TE and TM polarized light can be achieved even for a few periods of the quarter-wave stack. Fig. 7 shows the angle dependence of a five-period SiO_2–Si_3N_4 DBR mirror for TE and TM polarizations. As an added advantage, the Si–SiO_2–Si_3N_4 material system offers monolithic integration of the polarization detectors with well-established VLSI circuitry implementing smart pixels and arrays for polarization sensing and imaging. The VCPD structures can be formed on Si VLSI circuits by depositing

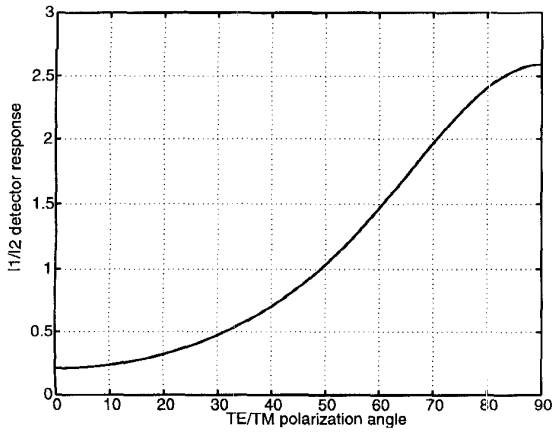

Fig. 8. The ratio of the current responses for detectors #1 and #2 for varying linear polarization angle. The incidence angle is Brewster's angle (for Si–air interface is 73.7°).

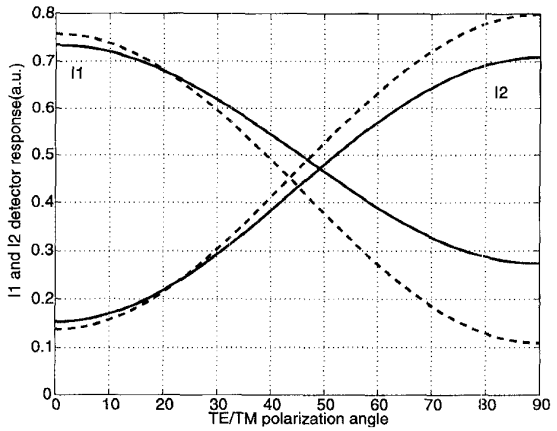

Fig. 9. The current responses for detectors #1 and #2 for varying linear polarization and incidence angle. Current responses for two different incidence angles are displayed: Brewster's angle (solid line) and an angle of 60° (dashed line).

dielectric films for DBR mirrors and using LPCVD (liquid-phase chemical-vapor deposition) to deposit polycrystalline Si for the top absorption layer in the RCE detector. However, the VLSI circuitry would have to be carefully monitored due to the high temperature of the LPCVD process. The VLSI circuit can be accessed by mesa processing of the detector structure and detectors can be integrated with electronic devices for processing of the two detector outputs to compute the incident polarization. The optical and electrical properties of Si allow for fabrication of polarization detectors in visible to near-IR wavelength range [10]. For MO storage applications, the capability of fabricating polarization sensors in the visible spectrum is particularly important since the storage capacity scales inversely with the wavelength. As an example, the absorption coefficient for poly-Si at an operation wavelength of 632 nm is in the mid 10^4 range, which was calculated to yield a 70% quantum efficiency for the RCE detector.

For both the VCPD and the multielement polarization detector, the detector responses (currents) I_1 and I_2 can be expressed as

$$\begin{bmatrix} I_1 \\ I_2 \end{bmatrix} = \begin{bmatrix} S_{1,\mathrm{TE}} & S_{1,\mathrm{TM}} \\ S_{2,\mathrm{TE}} & S_{2,\mathrm{TM}} \end{bmatrix} \cdot \begin{bmatrix} P_{\mathrm{TE}} \\ P_{\mathrm{TM}} \end{bmatrix} = [S] \cdot \begin{bmatrix} P_{\mathrm{TE}} \\ P_{\mathrm{TM}} \end{bmatrix} \quad (3)$$

where P_{TE} and P_{TM} are the incident power in corresponding polarizations, and $S_{i,\mathrm{TE}}$ and $S_{i,\mathrm{TM}}$ $(i = 1.2)$ represent the responsivity of the two detectors to different polarizations. Conventional notation for the responsivity R has been avoided to prevent confusion with mirror reflectivities. The $[S]$ matrix can be inverted and TE and TM powers can be evaluated from the detector currents as

$$\begin{bmatrix} P_{\mathrm{TE}} \\ P_{\mathrm{TM}} \end{bmatrix} = [S]^{-1} \cdot \begin{bmatrix} I_1 \\ I_2 \end{bmatrix}. \quad (4)$$

Equivalently, the ratio of the detector currents (I_1/I_2) can be used to evaluate the polarization of the incident light. Fig. 8 shows the calculated detector current ratio as a function of the polarization angle for a VCPD formed by the DBR described in Fig. 7 for an operation wavelength of $\lambda = 900$ nm. The polarization angle θ_p is defined as the angle between the electric field vector and the normal of the plane of incidence (Fig. 5), i.e., $P_{\mathrm{TE}} = \cos^2\theta_p$. The top detector (D_1) is formed by a 1.5-μm-thick Si absorber in RCE configuration and bottom detector (D_2) is assumed to detect all of the light transmitted through the DBR. The dependence of the detector current ratio to the polarization angle is a one-to-one correspondence. Therefore, the function can be inverted and polarization angle can be computed from measured detector current ratio. Basically, for a measured value on the y axis of Fig. 8, a unique polarization angle can be found by reading the corresponding value on the x axis. Thus, the resolution of the polarization sensing depends on the slope of the curve in Fig. 8. Fig. 9 displays the detector currents at two different incidence angles as a function of polarization. The cavity length of the RCE device is optimized separately for different incidence angle cases. The increase in the total variation of detector current ratio (I_1/I_2) observed at smaller incidence angles suggests improving polarization resolution. However, this improvement is accompanied by reduction in the linearity of the response. The authors would also like to mention that despite the fact that Fabry–Perot devices are very sensitive to temperature variations, we suspect that the VCPD's temperature sensitivity will be low. This is due to the small finesse and small cavity length ($\sim$2 μm).

V. Conclusion

We described a new technique for detecting the linear polarization of incident radiation by utilizing resonant cavity enhanced photodetectors and proposed two different device structures. These semiconductor devices represent an attractive substitute of bulk optical components such as polarization filters or beam splitters. The polarization sensitivity and optical detection functions are integrated into a single vertical device structure allowing for the monolithic fabrication of a polarization sensor. The Si–SiO_2–Si_3N_4 material system, for implementation of the vertical cavity polarization detectors,

has considerable advantages, such as high TE and TM polarization contrast and prospects of monolithic integration with VLSI circuits.

ACKNOWLEDGMENT

The authors would like to thank H. P. Zengingönül of the University of Illinois, and C. Feng, M. F. Ruane, and S. T. Dunham of Boston University for fruitful discussions.

REFERENCES

[1] K. Kaufmann, "Photodiodes advance optical storage devices," *Laser Focus World*, vol. 32, no. 2, pp. 109–112, Feb. 1996.
[2] T. Cronin, N. Shashar, and L. Wolff, "Imaging technology reveals the polarized light fields that exist in nature," *Biophoton. Int.*, pp. 38–41, Mar./Apr. 1995.
[3] L. W. Wolff and P. Costaines, "Polarization vision for object detection," *Proc. SPIE*, vol. 2103, pp. 106–114, 1994.
[4] J. Jahns and A. Huang, "Planar integration of free-space optical components," *Appl. Opt.*, vol. 28, no. 9, 1989.
[5] R. K. Kostuk, T.-J. Kim, G. Campbell, and C. W. Han, "Diffractive-optic polarization-sensing element for magneto-optic storage heads," *Opt. Lett.*, vol. 19, pp. 1257–1259, 1994.
[6] J. J. Kuta, H. M. van Driel, D. Landheer, and J. A. Adams, "Polarization and wavelength dependence of metal-semiconductor-metal photodetector response," *Appl. Phys. Lett.*, vol. 64, pp. 140–142, 1994.
[7] K. Kapser, P. P. Deimel, W. Platz, and U. Prechtel, "Platinumsilicide Schottky barrier infrared detectors with a grating: Dependence of the optical response on wavelength and polarization," *Appl. Phys. Lett.*, vol. 65, no. 2, pp. 1986–1988, 1994.
[8] M. S. Ünlü, B. M. Onat, H. P. Zengingönül, R. H. Henderson, and E. Towe, "Polarization sensitive photodetector arrays," in *Proc. Int. Semicond. Device Res. Symp.*, Charlottesville, VA, Dec. 1995.
[9] M. S. Ünlü and H. P. Zengingönül, "Polarization sensing with resonant cavity enhanced photodetectors," *Electron Lett.*, vol. 32, no. 6, pp. 591–593, 1996.
[10] M. S. Ünlü and S. Strite, "Resonant cavity enhanced (RCE) photonic devices," *J. Appl. Phys. Rev.*, vol. 78, no. 2, pp. 607–639, 1995.
[11] E. I. Chen, N. Holonyak, Jr., and S. A. Maranowski, "$Al_xGa_{1-x}As$–GaAs metal-oxide semiconductor field effect transistors formed by lateral vapor oxidation of AlAs," *Appl. Phys. Lett.*, vol. 66, no. 20, pp. 2688–2690, 1995.

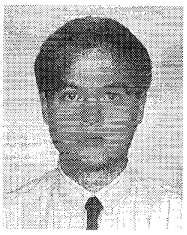

Bora M. Onat (S'92) was born in Melrose, MA, in 1971. He received the B.S. degree in electrical engineering from Istanbul Technical University, Turkey, in 1992, and the M.S. degree in electrical engineering from Boston University, Boston, MA, in 1995. He is currently working towards the Ph.D. degree at Boston University.

He received the Department of Education GAANN fellowship in January, 1996. His research interests include design, fabrication, characterization, and modeling of semiconductor optoelectronic devices.

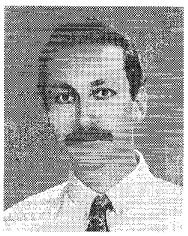

M. Selim Ünlü (S'90-M'92-SM'95) was born in Sinop, Türkiye, in 1964. He received the B.S. degree in electrical engineering from Middle East Technical University, Ankara, Türkiye, in 1986, and the M.S.E.E. and Ph.D. degrees in electrical engineering from the University of Illinois, Urbana-Champaign, in 1988 and 1992, respectively. His dissertation topic dealt with resonant cavity enhanced (RCE) photodetectors and optoelectronic switches.

From 1984 to 1986, he was a part-time Research Engineer with Military Electronics, Inc., Ankara, Türkiye, where he worked on VHF communication systems. In 1992, he joined the Department of Electrical and Computer Engineering, Boston University, Boston, MA, as an Assistant Professor. His current research interests include design, fabrication, characterization, and modeling of semiconductor optoelectronic devices, and near-field and picosecond spectroscopy.

During 1994–1995, Dr. Ünlü served as the Chair of IEEE Laser and Electro-Optics Society (LEOS), Boston Chapter, winning the LEOS Chapter-of-the-Year Award. He was also awarded the United Nations TOKTEN Award in 1995 and 1996. He is listed in American Men & Women of Science.